

# Planar Fiber-Optic Chips for Broadband Spectroscopic Interrogation of Thin Films

BROOKE M. BEAM, R. CLAYTON SHALLCROSS, JINUK JANG, NEAL R. ARMSTRONG,  
and SERGIO B. MENDES\*

Department of Chemistry, University of Arizona, Tucson, Arizona 85721 (B.M.B., R.C.S., J.J., N.R.A.); and Department of Physics and Astronomy, University of Louisville, Louisville, Kentucky 40292 (S.B.M.)

A planar fiber-optic chip (FOC) has been developed using side-polished optical fibers and characterized for broadband absorbance and fluorescence detection of molecular films. FOC technology combines the sensitivity of an attenuated total reflection (ATR) element with the ease of use of fiber-optic-based spectrometers and light sources to create an improved platform for spectroscopic analysis of molecular adsorbates. A multi-mode optical fiber (core diameter = 50  $\mu\text{m}$ , numerical aperture = 0.22, stepped refractive index profile) mounted in a glass V-groove block was side-polished to create a planar platform that allows access to the evanescent field escaping from the fiber core. For this generation of FOC technology, the exposed evanescent field has an interaction length of approximately 17.2 mm. The FOC platform was independently characterized through measurements of thin-film and bulk absorbing samples. The device performance was compared to the existing ATR technology and methods for increasing sensitivity of the FOC were investigated and validated. Additionally, we have demonstrated the ability of the FOC to both evanescently excite and collect fluorescence through guided modes of the optical fiber for a surface-confined luminescent semiconductor nanoparticle film (4 nm diameter, ligand capped, CdSe core). The FOC described here with a supported planar interface can facilitate the use of conventional planar deposition technologies and provide a robust planar platform that is amenable for incorporation into various sensor technologies.

Index Headings: Side-polished optical fiber; Attenuated total reflection spectroscopy; ATR spectroscopy; Absorbance; Fluorescence; Sensitivity; Nanoparticles.

## INTRODUCTION

New miniature, multifunctional, and sensitive sensor platforms are required for applications ranging from the characterization of photon-driven proton pumping in biomimetic photosynthetic devices,<sup>1</sup> sensing of drug/membrane protein interactions,<sup>2</sup> environmental contaminants,<sup>3</sup> and biological warfare agents.<sup>4</sup> In recent years, both planar waveguide-based and fiber-optic-based chemical sensors and biosensors have been developed in an attempt to meet the need for such device platforms.<sup>5–12</sup> Specifically, the planar single-mode integrated optical waveguide (IOW) structure can support the equivalent of about  $10^4$  reflections/cm of beam propagation, which provides an increase in absorbance sensitivity of 10 000 $\times$  compared to a conventional transmission measurement.<sup>13</sup> The planar single-mode IOW platform has been successful in several proof-of-concept demonstrations; however, its reduction to practice into an easy-to-use research tool for a broad audience of researchers has been difficult. A major hindrance for IOW technology has been interfacing the IOW chip with standard, commercially available spectroscopic

instrumentation. Optical coupling into and out of the IOW probing region requires precision optics, tight mechanical tolerances, advanced micro-optics fabrication technologies (e.g., integrated diffraction gratings), and time-consuming alignment of opto-mechanical components.<sup>9–11</sup> Although a fiber-optic device platform cannot fully reach the sensitivity provided by a single-mode IOW, it eliminates the difficulties related to the critical in- and out-coupling interfaces of an IOW by using standard fiber connections to sources and spectroscopic detectors. The advantages of using fiber-coupled spectroscopic platforms include portability, remote operation in harsh environments, and a large spectral region of optical transparency.<sup>5</sup>

The benefits of fiber-optic platforms have led several manufacturers of analytical instrumentation to develop inexpensive fiber-compatible equipment such as readily available fiber-coupled light sources and spectrometers, with standard distal end fiber coupling schemes. Previous studies that have taken advantage of the convenience of fiber-coupled instrumentation and the increased sensitivity of total internal reflection geometry have used a fiber optic with the cladding removed to create a sensing element around the cylindrical fiber core. The exposed core region serves as an attenuated total reflection (ATR) element that can be used for absorbance measurements to detect volatile organic compounds,<sup>14</sup> probe dye solutions,<sup>15</sup> monitor methane gas<sup>16</sup> and ammonium ion<sup>17,18</sup> concentrations, and determine solution pH using indicator-doped sol-gel coatings<sup>19,20</sup> or an indicator-doped polymer film.<sup>21</sup> Such fiber-optic sensor architectures employ signal transduction through a cylindrical probing interface, which can be problematic for several applications. Clearly, a supported planar interface would be advantageous for using standard planar deposition technologies such as Langmuir–Blodgett (LB) deposited thin films<sup>22,23</sup> and planar supported lipid bilayers.<sup>1</sup> In addition, due to its more robust supported platform, a planar design would be amenable for integration into microfluidic systems and sensor arrays. In this paper we investigate the optical performance characteristics for broadband absorbance and fluorescence spectroscopic applications of a chip-like planar waveguide platform formed by side-polishing an optical fiber embedded in the V-groove of a glass block; the planar waveguide device with transverse and lateral optical confinement is called here the fiber-optic chip (FOC) and is schematically shown in Figs. 1a and 2a.

Side-polished fiber technology has commonly been used in the optical telecommunication industry for the manipulation of light as wavelength filters, directional couplers, polarizers, and refractometers.<sup>24</sup> Comb filters and short-wavelength pass filters operate by picking off a particular wavelength of light where the effective refractive index of an overlay waveguide matches that of the fiber in which light is propagating.<sup>25,26</sup> Narrow band

Received 4 January 2007; accepted 14 March 2007.

\* Author to whom correspondence should be sent. E-mail: sbmend01@louisville.edu.

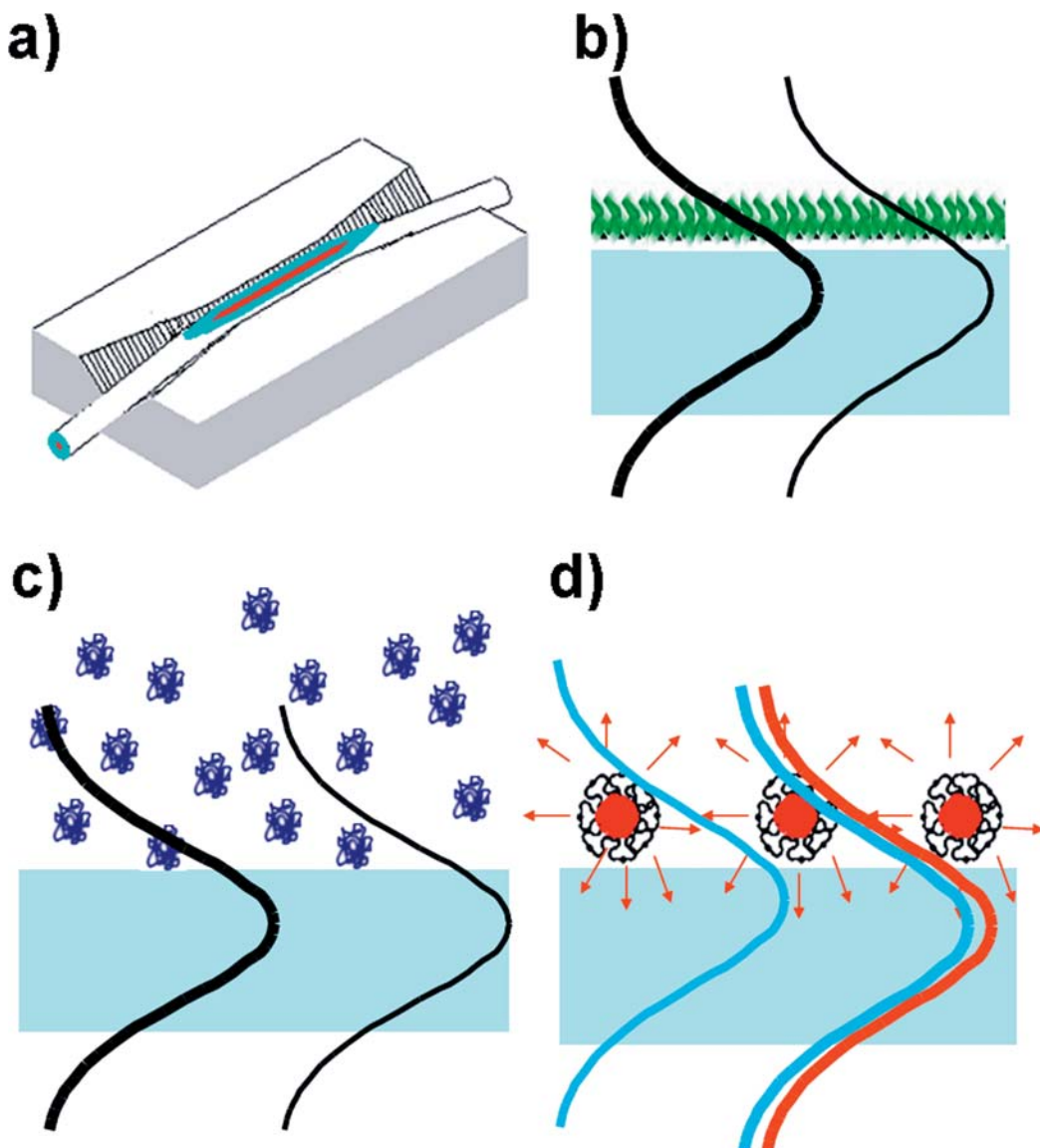


FIG. 1. (a) Schematic of the FOC showing a side-polished fiber imbedded in a glass V-groove from the top view. Different spectroscopic testing architectures for the FOC, where the black wave indicates guided broadband light. (b) Thin-film absorbance measurements using a polyelectrolyte P+/Ni(TSPc) bilayer. (c) Bulk absorbance measurements of an aqueous blue dextran solution. (d) Fluorescence back-coupling of a drop cast film of ligand capped CdSe nanoparticles (solid red circles), where the evanescent photons from the nanoparticles are indicated by the black waves emitted from the nanoparticles, the blue-green wave is the excitation wavelength, and the red wave is the back-coupled fluorescence.

filters use an intracore Bragg grating between two side-polished fibers to select the transmission of the wavelength of interest.<sup>27</sup> Bringing two side-polished fibers close enough together so that the light in the evanescent wave is guided by both fibers creates a tunable optical coupler, where the percentage of light carried through each arm of the coupler is dependent upon the distance between the two side-polished fibers.<sup>28</sup> Likewise, an all fiber polarizer can be constructed using a side-polished single-mode fiber with an overlay of a birefringent material.<sup>29,30</sup> Refractometers function similarly to optical filters and have been created using a direct liquid-to-fiber geometry,<sup>31</sup> sol-gel derived porous glass coatings,<sup>19</sup> Langmuir–Blodgett overlays,<sup>32</sup> polymer films, and metal films.<sup>33</sup>

Sensors based on refractive index changes in the overlay material of a side-polished fiber include detection of contaminated coconut oil,<sup>34</sup> water,<sup>35</sup> temperature,<sup>36,37</sup> and relative

humidity.<sup>38</sup> A side-polished fiber with a metallic film overlay can function as an in-line surface plasmon resonance (SPR) instrument that measures local refractive-index changes and has the advantage of simplified coupling optics.<sup>33</sup> Such an approach has been used for the measurement of salinity<sup>39</sup> and a biosensor that tests for staphylococcal enterotoxin B.<sup>40</sup> However, these previous side-polished fiber technologies are limited to monitoring only refractive index changes; it would be beneficial to utilize the side-polished fiber technology to yield more specific analytical information about the molecule of interest through broadband spectroscopic analysis.

There have been few side-polished fiber sensors created that utilize molecular absorbance of the evanescent wave. Gupta and Sharma constructed a pH dependent dye-doped sol-gel overlay waveguide that was shown to detect the pH of the superstrate solution from 2 to 13 pH units.<sup>41</sup> Additionally, a side-polished fiber biosensor has been reported using a colorimetric enzyme

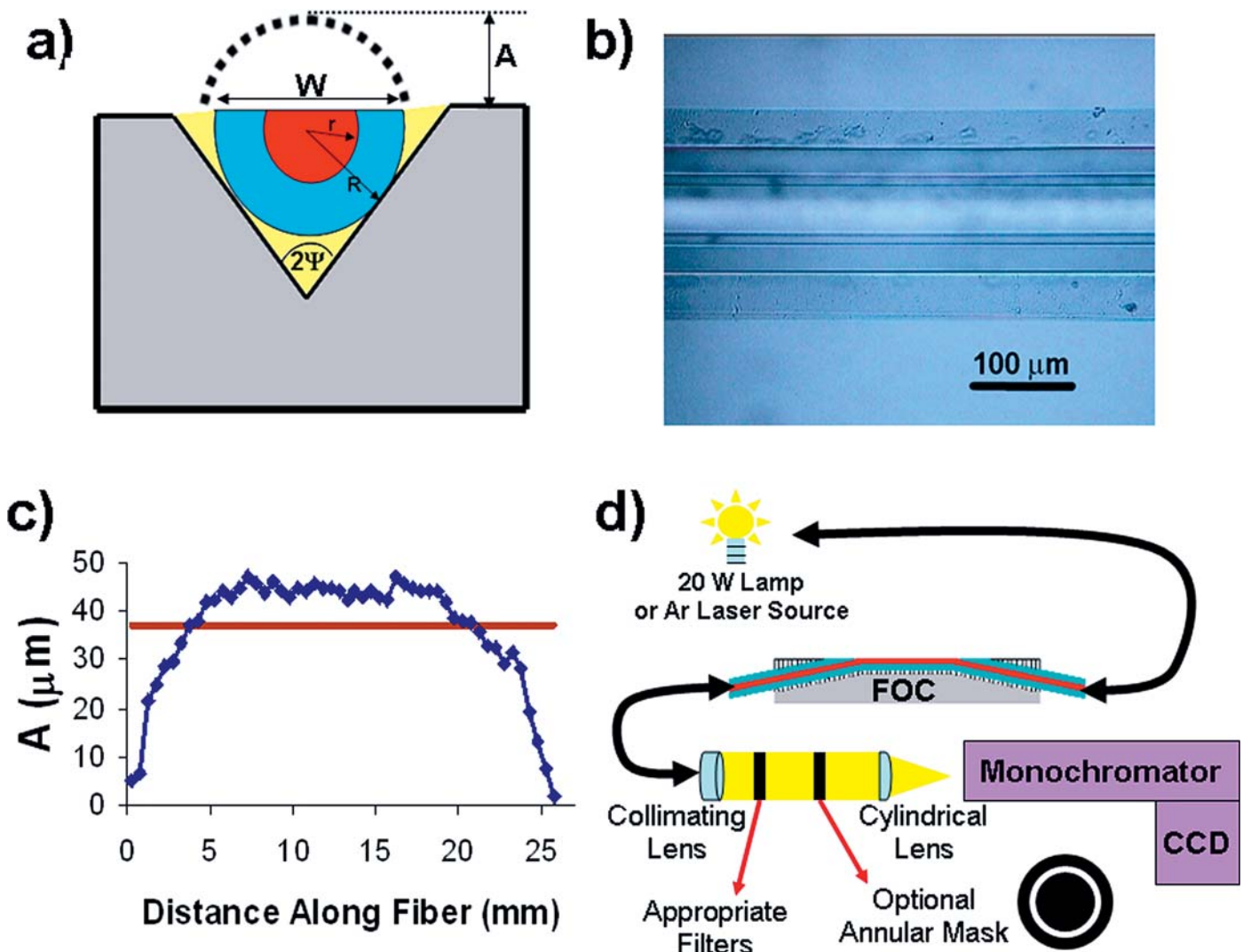


Fig. 2. Processing of the FOC: (a) schematic side view of a polished fiber where the depth, ( $A$ ), is calculated from measuring the width of exposed fiber ( $W$ ) and using  $R = 62.5 \mu\text{m}$ ,  $r = 25 \mu\text{m}$ , and  $\Psi = 35^\circ$ ; (b) microscope image (200 $\times$ ) of the polished surface of an FOC used to measure  $W$ ; (c) profile of the amount of fiber removed ( $A$ ) versus distance along the FOC (initial core height indicated by the red line), which gives an exposed core length of  $17.2 \pm 0.3 \text{ mm}$  and an estimated optical confining structure of  $40 \mu\text{m}$ ; and (d) experimental setup for the FOC, where either a fiber-coupled 20 W lamp or Argon laser can be used as a source. In the out-coupled beam, appropriate neutral density, band pass, long pass, and/or notch filters are placed orthogonal to the collimated beam. An optional annular mask was placed in the collimated out-coupled beam to conduct the masking experiments shown in Fig. 3c.

assay system to monitor the solution Penicillin G concentration with a detection range of 0 to  $0.4 \text{ mM}$ .<sup>42</sup> These sensor architectures have been limited to single wavelength detection, which is insufficient for many applications requiring broadband spectroscopic information; furthermore, they do not provide a systematic characterization of the device construction or a comparison with current analogous technology.

In this work the FOC device is characterized for both absorbance and fluorescence spectroscopies with a broad wavelength range of detection. The optical performance of the device is studied with both thin-film and bulk absorbing samples (Figs. 1b and 1c), and performance parameters are compared to conventional ATR spectroscopic platforms.<sup>43</sup> Next, methods for increasing the sensitivity of the FOC are investigated and validated. Our results precisely quantify the increased sensitivity provided by the FOC device due to the multiple reflections and, when compared to conventional ATR platforms, it offers the additional advantage of eliminating

complex coupling optics by using standard fiber-coupled sources and detectors. Finally, the FOC is used to demonstrate fluorescence back-coupling from adsorbates using a ligand capped CdSe semiconductor nanoparticle film (SC-NP) as a luminescent model system (Fig. 1d). This is a unique application of the FOC in as much as excitation and detection of the luminescent response is done entirely in-plane through guided modes, with no need for free-space optics or complicated alignment of the sensor element. Contrary to the unclad fiber approach, the FOC with a supported planar interface can facilitate the use of conventional planar deposition technologies (e.g., LB-deposited thin films) and provide a robust planar platform that is amenable for integration into various sensor architectures.

## EXPERIMENTAL

**Construction of the Fiber-Optic Chip.** A  $50 \mu\text{m}$  core diameter, step-index, multimode fiber with a  $125 \mu\text{m}$  cladding

diameter and a numerical aperture (NA) of 0.22 (Thorlabs AFS50/125Y) was used for all FOC devices described here. The bare fiber was mounted into a glass V-groove (Mindrum) using thermally curing epoxy (Epotek 301) (Figs. 1a and 2a), similar to that discussed in Tseng and Chen.<sup>24</sup> Prior to fiber mounting, the V-groove was depth corrected and the edges lapped at a 2° angle using a 10% w/w 19.5 μm aluminum oxide (Lapmaster) water solution. All lapping and polishing processes used a Lapmaster (model 12) lapping/polishing machine with a cast iron lapping plate covered in a polyurethane pad specific for each solution. The fiber-mounted device was then lapped at 20 rpm using 10% w/w 1 μm aluminum oxide (Lapmaster) water solution. The lapping depth of the device was monitored using a microscope (200×) with a calibrated charge-coupled device (CCD) camera (Motic 900), where the width of the polished fiber in the groove (W, Figs. 2a and 2b) was used to calculate the amount of the fiber removed (A, Fig. 2a). Once an appreciable amount of the fiber core was exposed ( $A > 37.5 \mu\text{m}$ ), a final polishing step at 30 rpm for one to two minutes using 5% w/w 0.5 μm cerium oxide (Logitech) water solution was used to complete the device, which had an average surface roughness of  $1.4 \pm 0.2 \text{ nm}$ , determined by atomic force microscopy (AFM, Digital Instruments Dimension 3100, tapping mode, Fig. S-1†). To determine the physical path length ( $L$ ) of the exposed core region, consecutive images were taken down the length of the polished fiber (Fig. 2b). Three measurements of exposed fiber width ( $W$ , tolerance of 2 μm) were made for each image and averaged; the average  $W$  is then used to calculate the amount of fiber removed ( $A$ ) for each image, which correlates to a fiber section with a length of 0.475 mm. The path length is then determined by the number of images with  $A$  greater than 37.5 μm and the tolerance assigned is half of the image length, which results in a path length of  $17.2 \pm 0.3 \text{ mm}$  for the FOC shown in Fig. 2c. In order to fiber couple the device, patch fiber cables were constructed with FC connectors (Fiber Instrument Sales) using the same type of fiber as in the FOC device. A patch fiber was spliced onto each end of the device fiber using a fiber fusion splicer (Ericsson FSU 995 FA).

**Experimental Layout and Protocols.** Before any measurements were made on the FOC, it was cleaned ultrasonically in 10% Alconox solution, rinsed with water, rinsed with ethanol, and blown dry with N<sub>2</sub>. A 20 W tungsten-halogen lamp (Phillips), which was focused into the fiber using a lens (Thorlabs; focal length, 25.4 mm; configuration, 1:1), was used as the light source for all broadband absorbance experiments (Fig. 2d). The other end of the FOC was fiber coupled into a monochromator (Acton SpectraPro 2150i) using a fiber collimating lens (Thorlabs; focal length, 11.0 mm) and a cylindrical lens (Thorlabs; focal length, 25 mm); appropriate filters and/or masks were placed between these two lenses and perpendicular to the beam of light. A CCD camera (Princeton PIXIS 400B) attached to the monochromator was used as a spectroscopic detection system for all absorbance and fluorescence experiments (Fig. 2d).

Masking experiments were performed with three different annular masks; each annular mask only allows a ring of light with a particular angle ( $n_{\text{air}} \sin \theta_{\text{air}} = 0.081 \pm 0.009, 0.116 \pm 0.009$ ,

and  $0.152 \pm 0.009$ ) and effective refractive index ( $N = 1.4577 \pm 0.0005, 1.4553 \pm 0.0007$ , and  $1.4521 \pm 0.0009$ ) to propagate, thereby selecting which fiber modes (i.e., internal angles) are used for probing the FOC interface.<sup>15</sup> The mask was placed after the neutral density filters and centered on the collimated beam of light before it was focused into the detector by a cylindrical lens (Fig. 2d). Additionally, the fiber exiting the FOC and entering the monochromator alignment optics was kept straight to prevent optical mode scrambling. The absorbance spectra collected with the masks are then compared to the absorbance spectra collected for the same film without a mask.

Conventional ATR spectroscopy was used to calculate the surface coverage for the determination of the sensitivity factor of the FOC for thin-film absorbance measurements. ATR measurements were made on a home-built instrument adapted from that previously reported by Doherty et al.<sup>43</sup> Instead of a Xe arc lamp, the source used was a 20 W tungsten-halogen lamp similar to that described above for coupling into the FOC. The detector used here was a commercially available fiber-coupled spectrometer (SI Photonics 430). Absorbance measurements of thin films were made on a glass slide, cleaned the same way as the FOC, and using TM polarized light; we measured a path length of 44 mm (10.6 reflections) and an angle (between the propagating beam and the waveguide normal) of 64° inside the glass substrate (Fig. S-2 and Table S-I).

Thin-film absorbance measurements were made using a polyion self-assembled film of poly(diallyldimethylammonium chloride) (P+) and nickel (II) phthalocyaninetetrasulfonic acid (Ni(TSPc)) using a dip-coating procedure.<sup>44,45</sup> A 1 wt % water solution of P+ (Aldrich, 20 wt % in water, high MW) was allowed to self assemble on the surface of the FOC for 15 minutes. Excess nonspecifically adsorbed polymer was rinsed off with water. Next, the P+ modified FOC was exposed to 1.0 mM Ni(TSPc) (Aldrich, tetrasodium salt) aqueous solution for 15 minutes to create a self-assembled P+/Ni(TSPc) bilayer film via electrostatic interactions. Excess Ni(TSPc) was rinsed away with water. All spectra are referenced to a transparent P+ film and water superstrate; therefore, the film absorbance is due only to adsorbed Ni(TSPc), which has an experimentally determined molar absorptivity of  $45\,550 \text{ M}^{-1} \text{ cm}^{-1}$  at 610 nm (Fig. S-3).

Blue dextran (Sigma) with an average molecular weight of 2 000 000 and a molar absorptivity<sup>46</sup> of  $1.8 \times 10^6 \text{ M}^{-1} \text{ cm}^{-1}$  at 633 nm was used to make aqueous solutions with concentrations of 10 μM, 12.5 μM, 15 μM, 20 μM, and 25 μM for bulk absorbance measurements. All spectra were referenced to a pure-water blank and smoothed using a five-point median method.

Fluorescence measurements were made on a thin-film of octadecylamine (ODA) capped CdSe SC-NPs drop cast from toluene. These SC-NPs were synthesized using a modified procedure from Peng et al. (see supplemental information, S-4).<sup>47</sup> The SC-NPs are excited by the 488 nm line from a fiber-coupled argon ion laser (Ion Laser Technologies, 25 mW). Collection of the SC-NP fluorescence was directly downstream of the source and filtered with two 488 nm notch filters (Edmund Optics and Kaiser) and a 550 nm long pass filter; the light was then coupled into the same spectroscopic detector previously described.

## RESULTS AND DISCUSSION

**Theory for the Thin-Film Sensitivity Calculation. Sensitivity Calculation with a Thin-Film Probe.** We first evaluated the sensitivity enhancement of the FOC device and

† All supplemental material mentioned in the text is available on the SAS homepage at [www.s-a-s.org](http://www.s-a-s.org). Supplemental material includes the following: S-1, AFM of lapped/polished surface of FOC; S-2, ATR study of the P+/Ni(TSPc) polyelectrolyte thin-film; S-3, determination of molar absorptivity for Ni(TSPc) solutions; S-4, synthesis of CdSe nanocrystals; and S-5, comparison of nanoparticle solution spectra with FOC spectra.

compared it to previously existing technologies. The sensitivity factor ( $S$ ) of a device, defined in Eq. 1, is a scaling factor of the device absorbance ( $A_{FOC}$ ) with respect to the conventional absorbance measured in direct transmission and used to quantify the sensitivity enhancement of the FOC and ATR platforms:

$$S \equiv \frac{A_{FOC,film}}{A_{trans}} = \frac{A_{FOC,film}}{\varepsilon_{film} \Gamma_{film}} \quad (1)$$

where  $\varepsilon$  is the molar absorptivity and  $\Gamma$  is the molecular surface coverage of the film under test.

The application of Eq. 1 requires the determination of the surface coverage, and for this purpose an independent ATR experiment on a glass slide was preformed. By using expressions adapted from Harrick<sup>48</sup> we have:

$$A_{ATR} = \varepsilon \Gamma r \left( \frac{n_l}{n_o \cos \theta_o} E_{TM}^2 \right) \quad (2)$$

$$E_{TM}^2 = \frac{4 \cos^2 \theta_o \left\{ \left[ 1 + \left( \frac{n_s}{n_o} \right)^4 \right] \sin^2 \theta_o - \left( \frac{n_s}{n_o} \right)^2 \right\}}{\left[ 1 - \left( \frac{n_s}{n_o} \right)^2 \right] \left\{ \left[ 1 + \left( \frac{n_s}{n_o} \right)^2 \right] \sin^2 \theta_o - \left( \frac{n_s}{n_o} \right)^2 \right\}} \quad (3)$$

where  $r$  is the number of geometrical reflections inside the ATR,  $n_o$  is the refractive index of the ATR substrate (1.51),  $n_s$  is the refractive index of the water superstrate (1.33),  $n_l$  is the refractive index of the Ni(TSPc) layer (which is assumed to be 1.7),<sup>49</sup>  $\theta_o$  is the waveguide angle inside the ATR substrate (64°), and  $E_{TM}^2$  is the relative electric field for TM polarized light in a thin film when the incident field has an amplitude of unity, as defined in Eq. 3. ATR absorbance measurements were made for three different bilayers adsorbed to the ATR platform, providing an average of  $\Gamma = 3.01 \times 10^{-10}$  mole/cm<sup>2</sup> (Fig. S-2 and Table S-I). By assuming that the surface coverage of the Ni(TSPc) film on the FOC device is the same as on the ATR substrate, we then calculated the sensitivity factor in the FOC by using Eq. 1 and the absorbance values measured for Ni(TSPc) films with an FOC device (Fig. 3a).

**Bulk Absorbance and Sensitivity Calculation.** In addition to the previous approach of using a thin-film sample adsorbed to the FOC surface for determining the sensitivity factor, we employed another method that consists of using the FOC device to measure the absorbance of a bulk absorbing sample, where no film is formed over the FOC surface and the absorbance is due to solution-dissolved chromophores. As shown in Ref. 53 (Eqs. 11–14), the sensitivity factor of a hypothetical thin film can be determined by measuring the solution absorbance of a non-specifically adsorbed dye, such as blue dextran, using Eq. 4:

$$S = \frac{A_{FOC,film}}{\varepsilon_{film} \Gamma_{film}} = \frac{A_{FOC,bulk}}{\varepsilon_{bulk} c_{bulk} \frac{\lambda}{4\pi(N^2 - n_s^2)^{1/2}}} \quad (4)$$

where  $N$  is the effective refractive index of the FOC fiber optic (here we use  $N = 1.46$  as there is only a very small difference in refractive index between the fiber core and cladding),  $n_s$  is the refractive index of the water solution (1.33), and  $\lambda$  is wavelength.

The absorbance for a series of blue dextran solutions (assumed

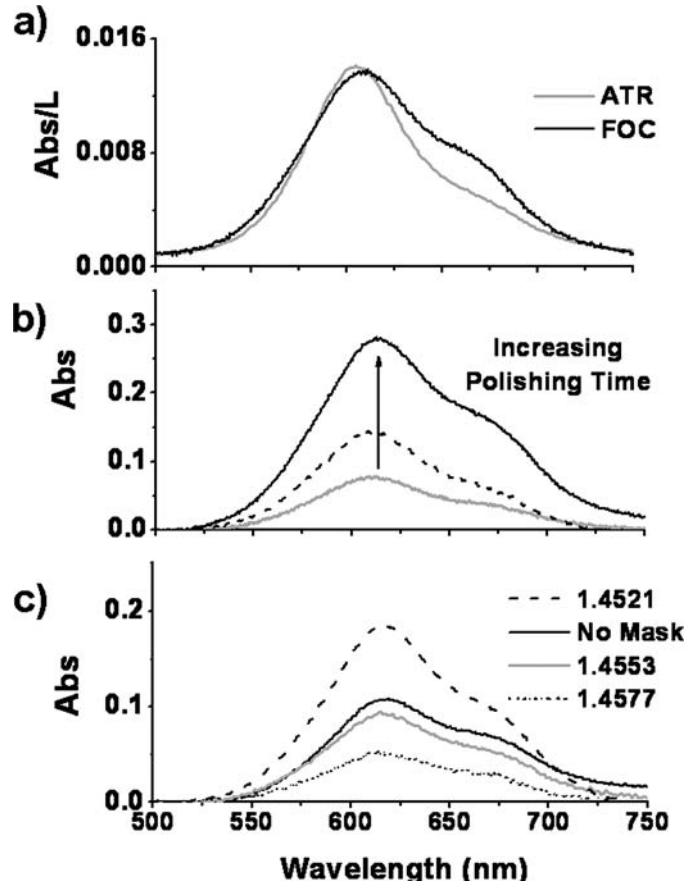
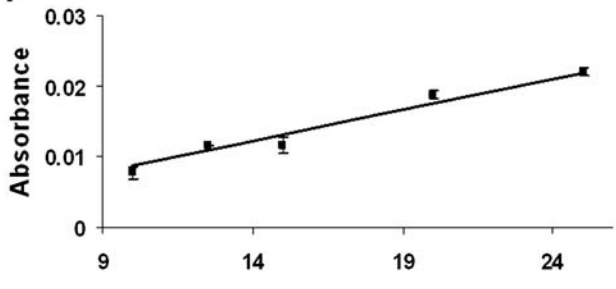


FIG. 3. All spectra are of a self-assembled polyion film of P+ and Ni(TSPc). (a) Comparison of thin-film sensitivity between ATR and FOC architectures; the spectra are normalized by their interaction lengths ( $L$ ) of 44 mm and 17.2 mm, respectively. (b) Increasing sensitivity of the FOC device for thin-film absorbance by adding a mechanical polishing step to the lapping process. FOC after lapping with 1  $\mu\text{m}$  aluminum oxide, where  $S = 6.2 \pm 0.2$  (grey line); FOC after polishing with 0.5  $\mu\text{m}$  cerium oxide for 1 min, where  $S = 13.0 \pm 0.4$  (dashed line); and FOC after 2 min of polishing, where  $S = 19.5 \pm 0.5$  (solid line). (c) Measured absorbance for the same sample film using different annular mask sizes (thus, different internal angles and effective indices of the light propagating within the FOC device) and no mask (solid line), where all of the modes of the FOC are equally illuminated. The results shown for the different masks are labeled by effective index ( $N$ ): 1.4577  $\pm$  0.0005 (dotted line), 1.4553  $\pm$  0.0007 (grey line), and 1.4521  $\pm$  0.0009 (dashed line). Absorbance is shown to increase as effective refractive index decreases.

to not specifically adsorb to the surface) was measured using the FOC. The slope of the linear plot of the FOC absorbance versus bulk concentration (Fig. 4a) was then related to  $S$  and compared to the sensitivity measured with the thin-film experiment.  $S$  calculated using either thin-film or bulk absorbance methods should be consistent for a particular FOC device and provide a means for comparison of  $A_{FOC}$  to absorbance measurements in a conventional transmission experiment.

**Physical Characterization of Fiber-Optic Chip Devices.** The sensitivity of an FOC device is intrinsically dependent upon the specific geometry of the side-polished fiber. The fundamental limit of the elliptical flattened area is determined by the structure of the V-groove mount, evenly mounting the fiber in epoxy, and the efficiency of exposure through the polishing process of the core region of the fiber. The length of the elliptical exposed core region is limited by the amount of V-groove removed to ensure that the sloping edge on both ends

a)



b)

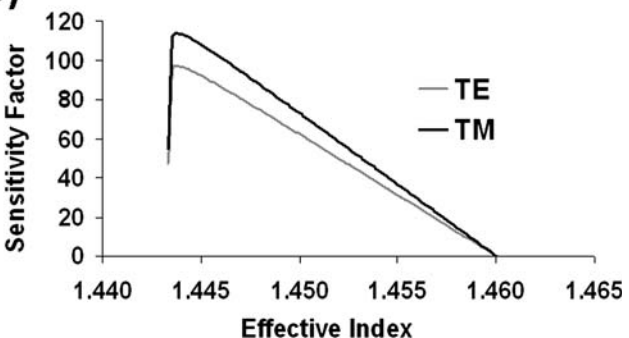


Fig. 4. (a) A calibration plot was made using the FOC detected absorbance at 633 nm of different bulk concentrations of blue dextran (10, 12.5, 15, 20, and 25  $\mu\text{M}$ ) in water. The linear regression gives a slope of  $0.00084 \pm 0.00002 \mu\text{M}^{-1}$  with a defined intercept of 0 to calculate the path length of  $4.68 \pm 0.01 \mu\text{m}$ , where  $S$  is calculated to be  $56 \pm 1$ . (b) Planar waveguide thin-film modeling calculation<sup>53,54</sup> of the sensitivity factor with respect to effective index for a waveguide with a thickness of 40  $\mu\text{m}$ , NA of 0.22, and probing length of 17.2 mm (average  $S = 49$ ).

of the support are low enough that the jacketed fiber will not protrude above the active area of the device, and the depth and angle of the groove itself. Therefore, there is an optimal polishing depth that defines the elliptical length and depends on each specific V-groove. The epoxy mounting step in the FOC fabrication is essential to ensure that the fiber is evenly mounted in the V-groove so that polishing the device provides a uniform planar waveguide area. To characterize each device, and to determine the possible evanescent wave interaction length, images were taken using a microscope and a calibrated camera down the entire length of the exposed ellipse to determine the possible evanescent wave interaction length. Figures 2a–2c illustrate this process for the FOC device used to collect the spectra in Fig. 3a, with an interaction length of  $17.2 \pm 0.3$  mm. The exposed evanescent field has an estimated interaction area of  $0.05 \text{ cm}^2$ . Further characterization of each device was carried out using AFM to determine the surface characteristics, where the polished chip used to collect the spectra in Fig. 3b has a root mean square (rms) surface roughness of  $1.4 \pm 0.2$  nm (Fig. S-1).

**Thin-Film Absorbance Measurements. Comparison of Fiber-Optic Chip and Attenuated Total Reflection Platforms.** The P+/Ni(TSPc) films were chosen to determine the sensitivity factor of the FOC devices for several reasons. The P+ modification layer was used because of its permanent positive charge, transparency, and ease of addition as a base layer to self-assembled poly-ion films.<sup>50</sup> The positively charged polymer adsorbs to the surface through electrostatic

interactions and provides ion-exchangeable groups for the Ni(TSPc) molecules.<sup>44,45,50</sup> Ni(TSPc) was chosen due to its ability to form stable, uniform, and highly absorbing films<sup>44</sup> with a solution molar absorptivity of  $45\,550 \text{ M}^{-1} \text{ cm}^{-1}$  at 610 nm, as confirmed from conventional ATR studies of these same films (see supplemental information, S-2 and S-3).

Figure 3a shows the normalized absorbance of a single P+/Ni(TSPc) bilayer on both the FOC (Fig. 1b) and ATR platforms, with path lengths of  $17.2 \pm 0.3$  mm (Fig. 2c) and 44 mm, respectively. The Q-band spectrum of the adsorbed Pc is blue-shifted relative to the absorbance seen for the non-aggregated monomer in solution.<sup>51</sup> Some absorbance is seen, however, for both platforms, near 680 nm, the  $\lambda_{\text{max}}$  for the monomeric species, and the relative concentration of this form is different for the two platforms. This suggests that there are slight differences in aggregation of Ni(TSPc) on the two platforms, which is most likely due to differences in surface composition of the substrate. The FOC platform has a more heterogeneous surface with the juxtaposition of bare silica fiber with the epoxy that holds it in place (Fig. 2b), while the ATR platform uses a more homogenous silica platform. The calculated sensitivity factor ( $S$ ) for the FOC is  $19.5 \pm 0.6$  and  $47 \pm 1.4$  for the ATR experiment. The FOC, however, yields a similar sensitivity enhancement versus that of the ATR measurement, illustrated by the overlapping peaks at the wavelength maximum in Fig. 3a when the spectra are normalized to correct for the difference in the physical path length. While the current generation of FOC technology discussed here has a sensitivity enhancement similar to the ATR system, its ease of use remains the major advantage over the use of prism-coupled ATR platforms. The FOC will “plug” into fiber-coupled sources and detectors, eliminating the time-consuming and tedious process of aligning in- and out-coupling optics for an ATR or waveguide.

**Enhancing Fiber-Optic Chip Thin-Film Absorbance Sensitivity.** Further refinements in the FOC platform promise to substantially increase its sensitivity. Two methods have been developed thus far that double the sensitivity of FOC devices: (1) additional mechanical polishing (Fig. 3b), and (2) masking the out-coupled light to eliminate the light from the fundamental modes of the fiber (Fig. 3c). Additional mechanical polishing of the FOC was accomplished using a 5% w/w 0.5  $\mu\text{m}$  cerium oxide slurry solution for different time periods, which serves to remove contaminants from the fiber surface and smooth the surface, only slightly increasing the exposed elliptical area. The surface roughness after lapping with a 1  $\mu\text{m}$   $\text{Al}_2\text{O}_3$  slurry was  $6 \pm 1$  nm and was improved via the cerium oxide polishing method to  $1.4 \pm 0.2$  nm (Fig. S-2). The additional polishing process on this FOC device resulted in increasing the sensitivity factor from an initial value of  $6.2 \pm 0.2$  for the freshly-lapped surface, to  $S = 19.5 \pm 0.5$  for cerium oxide polishing of the FOC for two minutes (Fig. 3b). This three-fold improvement is likely due to a cleaner and smoother FOC interface that allows an enhanced analyte surface coverage and reduces light scattering of higher order modes, which have stronger interaction with adsorbed films (as experimentally shown in the next paragraph).

The lower order modes of a fiber (those with optical rays propagating at a small angle from the fiber axis and described by a greater effective refractive index,  $N$ ) do not provide a strong interaction with the molecules adsorbed on the active surface of the FOC. Removing these lower order modes from

the optical beam prevents collecting average absorbance measurements that are unduly weighted toward the less sensitive traveling waves inside the fiber.<sup>52</sup> To select the modes allowed to propagate in the FOC, an annular mask that only transmits a ring of light of a defined angle was used (Fig. 2d).<sup>15</sup> Figure 3c compares the absorbance spectra of the same P+/Ni(TSPc) film taken using the FOC with no mask (all modes present) to three different annular masks defined by effective refractive index ( $N = 1.4577 \pm 0.0005$ ,  $1.4553 \pm 0.0007$ , and  $1.4521 \pm 0.0009$ ). There is an inverse relationship between the effective refractive index and absorbance as shown by the spectra for the different masks in Fig. 3c. This same trend is confirmed by the modeling calculations for the sensitivity factor across all modes (or  $N$ ) of a slab waveguide, discussed in the next section (Fig. 4b). By using a mask with a low  $N$  (1.4521), therefore working only with the highest order modes that the fiber can support, the absorbance is almost double compared to that measured for the same film without a mask.

**Bulk Absorbance Measurements.** Blue dextran was used for bulk absorbance measurements because it is nonionic and thus is assumed not to specifically adsorb to the surface of the FOC (Fig. 1c). Figure 4a contains the results of a set of experiments in which the absorbance of different concentrations of blue dextran solutions (10, 12.5, 15, 20, and 25  $\mu\text{M}$ ) was measured using the FOC. A narrow range of solution concentrations was tested in these experiments because of the limitations imposed by the signal-to-noise ratio and the maximum obtainable solution concentration. The plot of FOC absorbance versus bulk concentration in Fig. 4a is linear, confirming that blue dextran is not significantly adsorbing to the surface. From the slope of the line (or the calculated solution path length of  $4.68 \pm 0.01 \mu\text{m}$ ), the sensitivity factor was determined to be  $56 \pm 1$ , whereas the sensitivity factor calculated from the thin-film measurements for the same FOC was  $19.5 \pm 0.6$ , a multiple of 2.9 times lower. To further validate the experimentally calculated sensitivity factor, modeling calculations were carried out. Figure 4b shows a plot of the theoretically calculated sensitivity factor versus effective refractive index that varies linearly between 0 and 101 for different values of the effective index, where the effective index is an expression of the modes supported by the waveguide. This plot is an expansion of planar waveguide modeling work previously reported,<sup>53,54</sup> where the modeling parameters were as follows: 40  $\mu\text{m}$  waveguide thickness, 17.2 mm interaction length, and an NA of 0.22. When all fiber modes are equally excited, we should take the average of their individual responses for both TM and TE polarized light, giving  $S = 49$ , which agrees well with the experimentally calculated sensitivity factor from bulk measurements of 56.

The sensitivity factor obtained using the bulk measurements more accurately represents the actual device performance than the thin-film measurement. This discrepancy can be partially due to the assumption that the surface coverage of the P+/Ni(TSPc) thin-film on the FOC surface is the same as that on the ATR glass surface. As previously shown, the Ni(TSPc) molecules have an increased Ni(TSPc) monomeric concentration on the FOC over that of the ATR (Fig. 3a), which suggests differences in the microstructure of the films formed on the two testing platforms.

**Fluorescence Collection of Surface-Confining SC-NPs.** Thus far we have characterized and optimized the FOC as an

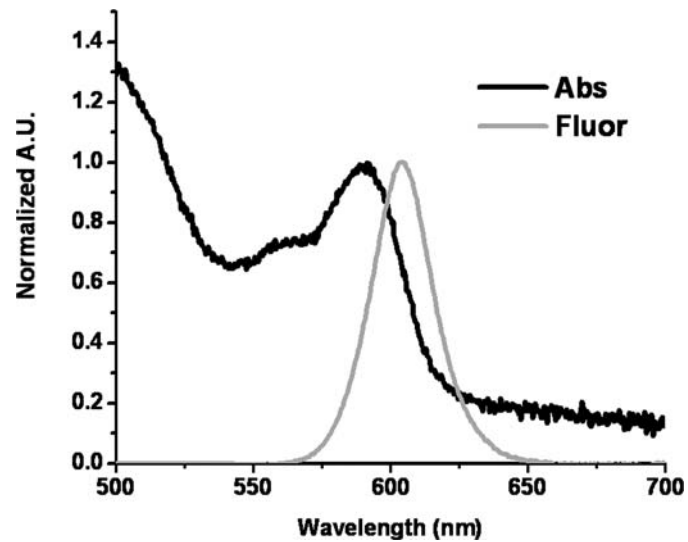


FIG. 5. Sequential measurements of absorbance and back-coupled fluorescence spectra using an FOC device for a drop cast film of CdSe ODA-capped nanoparticles, which have a calculated average diameter of  $4.13 \pm 0.01 \text{ nm}$  and surface coverage of about seven monolayers ( $8.94 \times 10^{-11} \text{ mole/cm}^2$ ). Both spectra are graphed using arbitrary units normalized to the absorbance and fluorescence peak maximum with respect to wavelength.

absorbance spectroscopic platform; however, it is essential for a spectroscopic device to function using several detection schemes. To increase the multifunctionality of the FOC device, we explored its capabilities as a fluorescence detection platform, which is especially important in sensor applications. A drop cast film of SC-NPs was chosen as the test system for fluorescence measurements due to the high molar absorptivity, sharp luminescence, and high fluorescence quantum yield of these nanoparticles. The absorption maximum and subsequent fluorescent peaks in ligand-capped semiconductor nanoparticles are due to the size-dependent quantum confinement of the nanocrystals, which has been previously discussed.<sup>55–57</sup> Figure 5 shows the results of sequential measurements on the FOC of absorbance and fluorescence for a drop cast film of ODA capped CdSe nanoparticles (Fig. 1d), which correlates with that of the spectra collected in solution (Fig. S-4). The film is made up of SC-NPs with a calculated diameter of  $4.13 \pm 0.01 \text{ nm}$ <sup>58</sup> and a surface coverage of about seven monolayers or  $8.94 \times 10^{-11} \text{ mole/cm}^2$ .

This is a unique application of the FOC in as much as excitation and detection of the luminescence response is done entirely in-plane and illustrates the ability to collect the fluorescence of the SC-NP film in a lower refractive index medium (in this case air  $n = 1.00$ ) through guided modes of the FOC device. According to Snell's law, light traveling from a lower refractive index medium is refracted at angles below the critical angle in the high-index medium and thereby cannot be guided. However, due to the proximity of the fluorophores to the guiding structure of the FOC (Fig. 1d), the evanescent photons, or electromagnetic field created by the oscillation of the excited dipole from those fluorophores, overlap with the evanescent tail of the fiber modes and meet the conditions for light propagation within the waveguide, as was predicted by Carniglia, Mandel, and Drexhage.<sup>59</sup> A related platform using a bent configuration of a single-mode fiber to collect the luminescence of rhodamine 6-G has been previously reported; however, this device was limited to single wavelength

detection and relied on frequency modulated detection.<sup>60</sup> The ability to simply collect broadband fluorescence will enable the FOC device to be used in a broad range of sensor configurations using fluorescence detection systems, including on-chip, fully integrated excitation and sequential optical characterization of luminescent analytes.

## CONCLUSION

A multi-mode side-polished fiber device has been created for use in absorbance and fluorescence spectroscopies. Absorbance measurements were made on P+/Ni(TSPc) polyion thin films and blue dextran bulk solutions, and the FOC was shown to have a sensitivity factor of 19.5 from thin-film measurements and 56 from bulk solution measurements. Modeling calculations indicate that the thin-film sensitivity should be 49, which is consistent with the bulk solution experiment. Currently, the FOC yields thin-film absorbance values comparable with ATR instrumentation; however, it eliminates the complex coupling optics and alignment procedures required to make such measurements. In addition, improving the polishing of the FOC surface and using higher order modes were shown to double the thin-film absorbance measurements. The FOC can serve as a planar support for molecular films such as lipid bilayers, which have applications for a variety of sensors. Finally, we have demonstrated the ability to simply guide back-coupled fluorescence into the FOC from a drop cast film of SC-NPs, broadening the potential applications of this technology to include sensor architectures that require fluorescence signal transduction. Future work on further developing the FOC technology will be focused on broadening the wavelength range into the ultraviolet, exploring the use of an FOC as a spectroelectrochemical platform, combining multiple FOCs together into a scalable array, and testing chemical and biochemical sensor schemes.

## ACKNOWLEDGMENTS

This work was supported by the National Science Foundation under Grants Number DBI-0352449, CTS-0428885, and CHE-0517963 and the Science and Technology Center—Materials and Devices for Information Technology Research Grant Number DMR-0120967. B.M.B. acknowledges fellowship support from a TIRF Proposition 301 (Arizona) Graduate Fellowship in Photonics. The authors would like to thank Yevgeniy Merzlyak and Gary Paysnoe for their guidance on lapping and polishing procedures.

1. T. W. McBee, L.-Y. Wang, C. Ge, B. M. Beam, A. L. Moore, D. Gust, T. A. Moore, N. R. Armstrong, and S. S. Saavedra, *J. Am. Chem. Soc.* **128**, 2184 (2006).
2. R. W. Fitch and J. W. Daly, *Anal. Biochem.* **342**, 260 (2005).
3. M. L. Stegemiller, W. R. Heineman, C. J. Seliskar, T. H. Ridgway, S. A. Bryan, T. Hubler, and R. L. Sell, *Environ. Sci. Technol.* **37**, 123 (2003).
4. L. Song, S. Ahn, and D. R. Walt, *Anal. Chem.* **78**, 1023 (2006).
5. O. S. Wolfbeis, *Anal. Chem.* **78**, 3859 (2006).
6. R. A. Potyralio, S. E. Hobbs, and G. M. Hieftje, *Fresenius J. Anal. Chem.* **362**, 349 (1998).
7. D. J. Monk and D. R. Walt, *Anal. Bioanal. Chem.* **379**, 931 (2004).
8. B. Kuswandi, R. Andres, and R. Narayanaswamy, *Analyst (Cambridge, U.K.)* **126**, 1469 (2001).
9. T. E. Plowman, S. S. Saavedra, and W. M. Reichert, *Biomaterials* **19**, 341 (1998).
10. P. K. Tien, *Appl. Opt.* **10**, 2395 (1971).
11. J. T. Bradshaw, S. B. Mendes, and S. S. Saavedra, *Anal. Chem.* **77**, 29A (2005).
12. W. M. Reichert, *Crit. Rev. Biocompat.* **5**, 173 (1989).
13. S. B. Mendes, L. Li, J. J. Burke, J. E. Lee, D. R. Dunphy, and S. S. Saavedra, *Langmuir* **12**, 3374 (1996).
14. D. S. Blair, L. W. Burgess, and A. M. Brodsky, *Anal. Chem.* **69**, 2238 (1997).
15. V. Ruddy, B. D. MacCraith, and J. A. Murphy, *J. Appl. Phys.* **67**, 6070 (1990).
16. H. Tai, H. Tanaka, and T. Yoshino, *Opt. Lett.* **12**, 437 (1987).
17. R. A. Potyralio and G. M. Hieftje, *Appl. Spectrosc.* **52**, 1092 (1998).
18. C. Malins, M. Landl, P. Simon, and B. D. MacCraith, *Sens. Actuators, B* **51**, 359 (1998).
19. B. D. MacCraith, *Sens. Actuators, B* **11**, 29 (1993).
20. B. D. Gupta and D. K. Sharma, *Opt. Commun.* **140**, 32 (1997).
21. C. Egami, K. Takeda, M. Isai, and M. Ogita, *Opt. Commun.* **122**, 122 (1996).
22. W. J. Doherty, A. G. Simmonds, S. B. Mendes, N. R. Armstrong, and S. S. Saavedra, *Appl. Spectrosc.* **59**, 1248 (2005).
23. W. H. Flora, S. B. Mendes, W. J. Doherty, S. S. Saavedra, and N. R. Armstrong, *Langmuir* **21**, 360 (2005).
24. S.-M. Tseng and C.-L. Chen, *Appl. Opt.* **31**, 3438 (1992).
25. K. R. Sohn and J. W. Song, *Opt. Commun.* **203**, 271 (2002).
26. N.-K. Chen, S. Chi, and S.-M. Tseng, *Opt. Lett.* **29**, 2219 (2004).
27. N.-K. Chen, S. Chi, and S.-M. Tseng, *Jpn. J. Appl. Phys.* **43**, L475 (2004).
28. M. J. F. Digonnet and H. J. Shaw, *IEEE J. Quant. Electron.* **18**, 746 (1982).
29. R. A. Bergh, H. C. Lefevre, and H. J. Shaw, *Opt. Lett.* **5**, 479 (1980).
30. S.-P. Ma and S.-M. Tseng, *J. Lightwave Technol.* **15**, 1554 (1997).
31. K. T. Kim, K. H. Lee, S. Hwangbo, and K. R. Sohn, *Sens. Actuators, A* **126**, 335 (2006).
32. D. Flannery, S. W. James, R. P. Tatam, and G. J. Ashwell, *Appl. Opt.* **38**, 7370 (1999).
33. R. Alonso, F. Villuendas, J. Tornos, and J. Pelayo, *Sens. Actuators, A* **37–38**, 187 (1993).
34. M. Sheeba, M. Rajesh, C. P. G. Vallabhan, V. P. N. Nampoori, and P. Radhakrishnan, *Meas. Sci. Technol.* **16**, 2247 (2005).
35. K.-R. Sohn, K.-T. Kim, and J.-W. Song, *Sens. Actuators, A* **101**, 137 (2002).
36. W.-G. Jung, S.-W. Kim, K.-T. Kim, E.-S. Kim, and S.-W. Kang, *IEEE Photon. Technol. Lett.* **13**, 1209 (2001).
37. J. Senosiain, I. Diaz, A. Gaston, and J. Sevilla, *IEEE Trans. Instrum. Meas.* **50**, 1656 (2001).
38. A. Gaston, F. Perez, and J. Sevilla, *Appl. Opt.* **43**, 4127 (2004).
39. O. Esteban, M. Cruz-Navarrete, A. Gonzalez-Cano, and E. Bernabeu, *Appl. Opt.* **38**, 5267 (1999).
40. R. Slavik, J. Homola, and E. Brynda, *Biosens. Bioelectron.* **17**, 591 (2002).
41. N. K. Sharma and B. D. Gupta, *Opt. Commun.* **216**, 299 (2003).
42. E. E. Carlyon, C. R. Lowe, D. Reid, and I. Bennion, *Biosens. Bioelectron.* **7**, 141 (1992).
43. W. J. Doherty, C. L. Donley, N. R. Armstrong, and S. S. Saavedra, *Appl. Spectrosc.* **56**, 920 (2002).
44. X. Yang, S. Johnson, J. Shi, T. Holesinger, and B. Swanson, *Sens. Actuators, B* **45**, 87 (1997).
45. M. Lutt, M. R. Fitzsimmons, and D. Li, *J. Phys. Chem. B* **102**, 400 (1998).
46. D. R. Dunphy, S. B. Mendes, S. S. Saavedra, and N. R. Armstrong, *Anal. Chem.* **69**, 3086 (1997).
47. J. J. Li, Y. A. Wang, W. Guo, J. C. Keay, T. D. Mishima, M. B. Johnson, and X. Peng, *J. Am. Chem. Soc.* **125**, 12567 (2003).
48. N. J. Harrick, *Internal Reflection Spectroscopy* (Harrick Scientific, Ossining, New York, 1979).
49. D. Manno, R. Rella, L. Troisi, and L. Valli, *Thin Solid Films* **280**, 249 (1996).
50. D. Li, Y. Jiang, C. Li, Z. Wu, X. Chen, and Y. Li, *Polymer* **40**, 7065 (1999).
51. C. C. Leznoff and A. B. P. Lever, *Phthalocyanines: Properties and Applications* (VCH, New York, 1989).
52. D. Gloge, *Appl. Opt.* **10**, 2252 (1971).
53. S. B. Mendes and S. S. Saavedra, *Appl. Opt.* **39**, 612 (2000).
54. S. B. Mendes and S. S. Saavedra, *Opt. Exp.* **4**, 449 (1999).
55. C. B. Murray, D. J. Norris, and M. G. Bawendi, *J. Am. Chem. Soc.* **115**, 8706 (1993).
56. Y. Wang and N. Herron, *J. Phys. Chem.* **95**, 525 (1991).
57. L. Brus, *J. Phys. Chem.* **90**, 2555 (1986).
58. W. W. Yu, L. Qu, W. Guo, and X. Peng, *Chem. Mater.* **15**, 2854 (2003).
59. C. K. Carniglia, L. Mandel, and K. H. Drexlage, *J. Opt. Soc. Am.* **62**, 479 (1972).
60. P. Poscio, C. Depersinge, G. Vorin, B. Sheja, and O. Pariaux, *Sens. Actuators, A* **23**, 1092 (1990).